RSC Advances

PAPER

View Article Online
View Journal | View Issue

Cite this: *RSC Adv.*, 2018, **8**, 33993

Enhanced photocarriers separation of novel CdS/pt/Mo_2C heterostructure for visible-light-driven hydrogen evolution†

Xinbo Jing,[a] Xueying Peng,[a] Youzhi Cao,[a] Wei Wang*[a] and Shufen Wang*[b]

Received 26th June 2018
Accepted 12th September 2018

DOI: 10.1039/c8ra05473h

rsc.li/rsc-advances

The production of H_2 from water using photocatalysts is a promising way of generating clean, renewable and alternative energy. The key issue is to develop active and stable photocatalysts. Here, we report a novel CdS/Pt/Mo_2C heterostructure photocatalyst, where Pt nanoparticles are closely supported on CdS/Mo_2C. The UV-vis spectrum and EIS Nyquist plots show that Mo_2C can boost the absorption in the UV-vis region and improve the separation of the photogenerated electron–hole pairs from CdS. The Pt nanoparticles act as the active co-catalyst that promotes the transient photocurrent response. As a result, the CdS/Pt/Mo_2C photocatalyst exhibits an excellent H_2 evolution activity up to 1828.82 μmol h^{-1} g^{-1} under visible-light irradiation, 8.5 and 16.2 times higher than that of pristine CdS and CdS/Mo_2C, respectively. Moreover, a high apparent quantum yield (AQY) of 9.39% is obtained at 400 nm for the CdS/Pt/Mo_2C heterostructure photocatalyst.

1. Introduction

The cleanability and renewability of solar energy can be used to solve the problems of energy shortage and the environmental pollution, which are caused by the rapid development of global factories.[1–3] One of the most promising means to make full use of solar energy is photocatalytic water decomposition excited by semiconductor photocatalyst. In past decades, there have been considerable efforts to develop perfect semiconductor photocatalysts with high activities for water splitting.[4,5] However, there are still many limitations for us to promote the photocatalytic efficiency, for example, the low light absorption and the rapid recombination of photogenerated electron–hole pairs. Moreover, suitable photocatalysts with matched band gap positions and the stability necessary for overall water splitting are still lacking. Many semiconductors, such as TiO_2 and ZnO, mainly absorb UV light, which indicates that they use only about 4% of the solar spectrum.[6,7] To increase the visible-light response activity of semiconductors, many strategies have been reported, including doping,[8] coupling with other photocatalyst,[9] structure engineering,[10] and so on. Among all these strategies, a heterostructure is one way to simultaneously obtain both efficient charge separation and photo-electrochemical stability.[11]

For heterostructure photocatalysts, it is much important to select proper components. In recent years, many reports have shown that molybdenum carbides are active in a variety of catalytic reactions including desulfurization,[12] water–gas shift,[13] and hydrogenation reactions.[14–16] It has been proven that Mo_2C has excellent charge-transfer resistance.[17] However, research about molybdenum carbides mostly focus on electrocatalysts for hydrogen production. The investigations of molybdenum carbide applied as photocatalyst are rare and indistinct. At the same time, CdS is popular and promising material as it can be excited in the visible light region.[18] It has been proven that Pt is an excellent co-catalyst which can efficiently improve the photocatalytic H_2 evolution capacity of semiconductor photocatalysts.[19]

Here, we designed and synthesized a heterogeneous CdS/Pt/Mo_2C photocatalyst where the CdS acted as the photocatalyst, Pt as the photosensitizer[20] and Mo_2C as the electron-transfer mediator. The preparation process of CdS/Pt/Mo_2C is illustrated in Scheme 1. Powder active charcoal (PAC) and ammonium molybdate were used as the charcoal and molybdenum source to synthesize tubular Mo_2C in Ar atmosphere. Pt nanoparticles were synthesized by photodeposition method. Then, Pt nanoparticles were deposited on CdS, which was synthesized by a typical chemical bath deposition process. CdS/Pt/Mo_2C photocatalyst is an efficient photocatalyst for H_2 production under visible-light irradiation. The CdS/Pt/Mo_2C samples exhibit enhanced visible-light absorption and excellent H_2 evolution performance compared to pristine CdS and CdS/Mo_2C. The superior performance of CdS/Pt/Mo_2C is outstanding when compared with previously developed photocatalysts.[11,21–23] A possible mechanism was also put forward

[a]*School of Chemistry and Chemical Engineering, Key Laboratory for Green Processing of Chemical Engineering of Xinjiang Bingtuan, Shihezi University, Shihezi 832000, China*

[b]*College of Sciences, Shihezi University, Shihezi 832000, China*

† Electronic supplementary information (ESI) available. See DOI: 10.1039/c8ra05473h

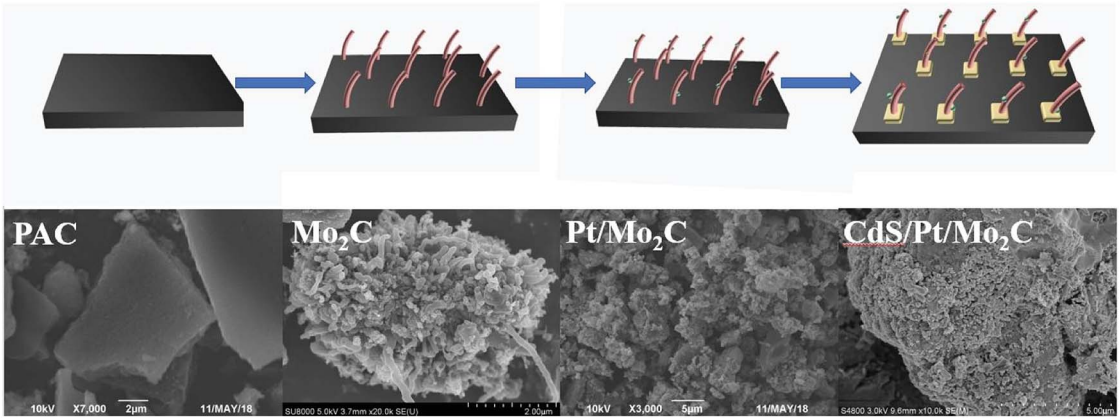

Scheme 1 Schematic of the preparation process of CdS/Pt/Mo_2C heterostructure.

to explain the improved photocatalytic performance of the heterogeneous catalyst.

2. Experimental

2.1 Materials

All the chemicals in the experiments were of analytical reagent grade and used without further purification. Ammonium molybdate ($(NH_4)_6Mo_7O_{24}\cdot 4H_2O$), hexamethylenetetramine ($C_6H_{12}N_4$), active charcoal powder, cadmium nitrate tetrahydrate ($Cd(NO_3)_2\cdot 4H_2O$), and Na_2S, chloroplatinic acid hexahydrate ($H_2PtCl_6\cdot 6H_2O$) were purchased from Sinopharm Chemical Reagent Co., Ltd, China.

2.2 Sample synthesis

Synthesis of Mo_2C. Mo_2C was synthesized by a typical calcination method as follows: 1 g ammonium molybdate ($(NH_4)_6Mo_7O_{24}\cdot 4H_2O$) and 226.9 mg hexamethylenetetramine ($C_6H_{12}N_4$, molar ratio almost is 1 : 2) were dissolved in 20% $NH_3\cdot H_2O$ (7 mL). Then, 0.2 g active charcoal powder was added into the solution. The suspension was then further homogenized in an ultrasonic bath for 40 min. The slurry was dried at room temperatures for 24 h. The sample was vacuum-dried for 12 h at 60 °C. For carburization, the solid mixture was annealed in a tube furnace under Ar flow at 100 mL min^{-1} from ambient to 800 °C at a rate of 2 °C min^{-1} and then held at 800 °C for 2 h. Ar was kept purging through the reactor while it was cooled to ambient temperature.

Synthesis of Pt/Mo_2C. Pt/Mo_2C was synthesized by a typical photodeposition method. Typically, 400 mg Mo_2C with different mass fractions of chloroplatinic acid hexahydrate ($H_2PtCl_6\cdot 6H_2O$) was dissolved in 30 mL deionized water to form a black slurry solution under magnetic stirring at room temperature. The suspension was stirred for 24 h in the dark to achieve the preferential adsorption of Pt based complex ions and then exposed to ultraviolet light (300 W Xe lamp without a cutoff filter of 400 nm) for 3 h to reduce the Pt based complex ions to Pt nanoparticles. After the photodeposition, the dark Pt/Mo_2C product was collected by centrifugation and washed with deionized water several times to remove dissolvable ionic impurities. The sample was vacuum-dried at 60 °C overnight. The mass fraction of Pt to Mo_2C was fixed as 0.5%, 1%, 3% (namely, mass fraction Pt/Mo_2C = 0.5%, 1%, 3%) and obtained products were named as Pt/Mo_2C-0.5, Pt/Mo_2C-1, and Pt/Mo_2C-3, respectively.

Synthesis of CdS/Mo_2C, CdS/Pt/Mo_2C or CdS. CdS/Mo_2C, CdS/Pt/Mo_2C or CdS were synthesized by a typical chemical bath deposition. 400 mg of Mo_2C or Pt/Mo_2C sample was added in 50 mL water containing 19.605 mL cadmium nitrate tetrahydrate ($Cd(NO_3)_2\cdot 4H_2O$, 0.1 M), and the solution was then stirred for 0.5 h in the dark to achieve the preferential adsorption of Cd based complex ions. 20 mL of 0.1 mol L^{-1} Na_2S solution was added drop wise into the suspension under vigorous stirring at room temperature. The resulting suspension was continually stirred at room temperature for 2 h and kept overnight. The CdS product (CdS/Mo_2C, or CdS/Pt/Mo_2C) was collected by centrifugation and washed with deionized water several times to remove dissolvable ionic impurities. The sample was vacuum-dried at 60 °C overnight. After the product was ground into powder, the resulting product was calcined at 550 °C for 4 h under Ar gas flow. In addition, pure CdS was also obtained through the similar chemical bath process without introducing Mo_2C. The obtained products were named as CdS/Pt/Mo_2C-X, that is, CdS/Pt/Mo_2C-0.5, CdS/Pt/Mo_2C-1, CdS/Pt/Mo_2C-3.

2.3 Photocatalytic hydrogen evolution

The photocatalytic hydrogen evolution reactions were conducted in a side-irradiation Pyrex reactor which was connected to a glass-closed gas circulation system at ambient temperature. In a typical photocatalytic experiment, 50 mg of catalyst power was suspended in 100 mL aqueous solution containing Na_2S (0.1 M) and Na_2SO_3 (0.1 M) as the sacrificial agent for hole scavenging. Before visible light irradiation, the reactant system was degassed by evacuation to remove air and ensure that the reaction system was under anaerobic conditions. It was then was irradiated by a 300 W Xe lamp with a cutoff filter of 400 nm for H_2 evolution under magnetic stirring. The amount of hydrogen evolution was analyzed by an online gas chromatograph (Agilent 7890, TCD, Ar as carrier).

The apparent quantum yield (AQY) for photocatalytic H_2 production was calculated as follows:

$$\mathrm{AQY} = \frac{2 \times \text{number of evolved hydrogen molecules}}{\text{number of incident photons}} \times 100\%$$

The number of incident photons were measured by a calibrated Si photodiode (SRC-1000-TC-QZ-N, Oriel, USA), and the distance between the calibrated Si photodiode and Xe-lamp with a 400 nm filter was 10 cm.

2.4 Electrochemical measurements

Photo-electrochemical measurements were performed on an electrochemical analyzer (Chenhua CHI 660) in a standard three-electrode cell. The working electrodes were prepared by drop-coating homogeneous catalyst suspensions directly onto the precleaned indium tin oxide glass (ITO glass) surfaces (1×2 cm). Samples on ITO glass with an active area of *ca.* 1×1 cm (1 mg of photocatalyst) were prepared as the working electrode. Platinum wire was used as the counter electrode, and a saturated calomel electrode (SCE) was used as the reference electrode. The E^0 is 0.241 V *vs.* NHE at 25 °C for a saturated calomel electrode. Na_2SO_4 (0.5 M) aqueous solution was used as the supporting electrolyte. Electrochemical impedance spectroscopy (EIS) plots were collected at the open circuit potential (0.5 V *vs.* SCE), with the frequency ranging from 100 kHz to 0.01 Hz and modulation amplitude of 5 mV. The transient photocurrent measurements were recorded at an applied potential of 0.5 V *vs.* SCE under visible light illumination. A 300 W Xe lamp equipped with an optical cutoff filter of 400 nm was employed for the visible-light excitation.

2.5 Characterizations

Powder X-ray diffraction (PXRD) data were collected using a Bruker AXS D8 X-ray diffractometer using Cu Kα radiation (λ = 1.54056 Å). Scanning electron microscope (SEM) images were recorded with a JEOL JSM-6490LV. Transmission electron microscope (TEM) and high-resolution transmission electron microscope (HRTEM) images were obtained by using a FEI Tecnai G2. The photocurrent response curves (PR) and electrochemical impedance spectroscopy (EIS) plots were collected by a CHI 660 electrochemical analyzer. Chemical states of the obtained samples were characterized by an Escalab 250 Xi system (a monochromatic Al Kα X-ray radiation). The binding energies of all elements were calibrated by the C 1s peak at 284.6 eV. UV-vis spectra were collected using a Thermo Fisher spectrometer with $BaSO_4$ as a reference. The photoluminescence (PL) spectra were taken on a FLS 980 fluorescence spectrometer with an excitation wavelength of 318 nm.

3. Results and discussion

As showed in Fig. 1a, similar and sharp diffraction peaks (Fig. 1a) of the as-prepared CdS/Pt/Mo_2C-0.5, CdS/Pt/Mo_2C-1 and CdS/Pt/Mo_2C-3 (the names are explained in 2.2 Sample synthesis) indicate excellent crystallinity. Fig. S2† shows the XRD pattern of CdS/Pt/Mo_2C-0.5. The five characteristic peaks at 37.76°, 43.69°, 63.39°, 75.72° and 79.86° belonging to (111), (200), (220), (311) and (222) plane can be assigned to molybdenum carbide (JCPDS 77-0720). At the same time, five diffraction peaks at 2θ values of 24.80°, 26.50°, 28.18°, 36.62°, 52.79° correspond to the (100), (002), (101), (102) and (201) planes in CdS (JCPDS no. 77-2306), respectively. It is noteworthy that the diffraction peaks of CdS/Pt/Mo_2C-0.5 are weaker than those of the other five samples, suggesting the relatively lower crystallinity. The XRD pattern of Mo_2C and CdS correspond well with orthorhombic Mo_2C phase (JCPDS no. 77-0720) and hexagonal CdS (JCPDS no. 77-2306), respectively. The XRD patterns of CdS/Pt/Mo_2C-0.5 (Fig. S1†) are analogous to that of CdS/Mo_2C, but no peaks for Pt can be observed. This is because of the relatively low concentration and relatively small size of Pt nanoparticles,[24] which can be confirmed by the full XPS survey spectrum of CdS/Pt/Mo_2C-0.5 (Fig. S3a†).

To investigate the morphology of the CdS/Pt/Mo_2C-0.5 sample, scanning electron microscope (SEM) measurements were performed. From the SEM (Fig. 1b), it can be seen that CdS is closely connected with Mo_2C and covers the surface of the active charcoal powder, as confirmed by EDS (Fig. S5†), the elemental mappings and TEM (Fig. S5†). The photodeposited Pt closely interacted with the CdS and Mo_2C to form a CdS/Pt/Mo_2C triphase structure (Fig. 1c). The lattice spacing with distances of 0.226 nm, 0.336 nm and 0.207 nm originated from Pt (111), CdS (002) and Mo_2C (200) planes, respectively and are consistent with the XRD results. TEM and HRTEM images of the CdS/Pt/Mo_2C-0.5 sample reveal that rather than a simple physical mixture, Pt and Mo_2C, and CdS and Mo_2C are in close contact, and form actual interfaces with each other, indicating the successful synthesis of a heterojunction.

The triphase heterojunction structure leads to a change of valence state and electron density of Cd, Mo and Pt. In order to further ascertain the details of the surface chemical composition and valence state of the CdS/Pt/Mo_2C system, the XPS spectrum of the CdS/Pt/Mo_2C-0.5 was measured (Fig. S3†). The full XPS spectrum of CdS/Pt/Mo_2C-0.5 (Fig. S3a†) shows S, Mo, C, O, and Cd with sharp peaks. These results correspond to the EDS (Fig. S5†). At the same time, the weak peak of Pt is found at a binding energy of 71.78 eV (Fig. S3c†), suggesting that Pt exists in the oxidation state, Pt^0. The XPS peaks of Cd 3d (Fig. S3e†) and Mo 3d (Fig. 1d) match well with those in previous studies. The peak fitting suggests oxidation states of Cd^{2+} for Cd and Mo^{2+} and Mo^{4+} for Mo. The binding energies of the Mo $3d_{5/2}$ and Mo $3d_{3/2}$ peaks were 228.2 and 231.4 eV, respectively and are typical values for Mo^{2+} in Mo_2C. The high resolution XPS data of S 2p exhibits two peaks at 162.24 eV and 163.37 eV (Fig. S3b†), which can be assigned to S $2p_{3/2}$ and S $2p_{1/2}$, respectively. In addition, there is a distinct peak of 169.63 eV in the high resolution XPS of S 2p, which can be distributed to SO_4^{2-} that may be created during the process of calcination. The XPS results confirm the existence of CdS, Mo_2C and Pt.

For photocatalysts, the most important question is to lower the recombination of photogenerated electron–hole pairs. Photoluminescence (PL) spectroscopy was performed to confirm the capability of the samples in separating the

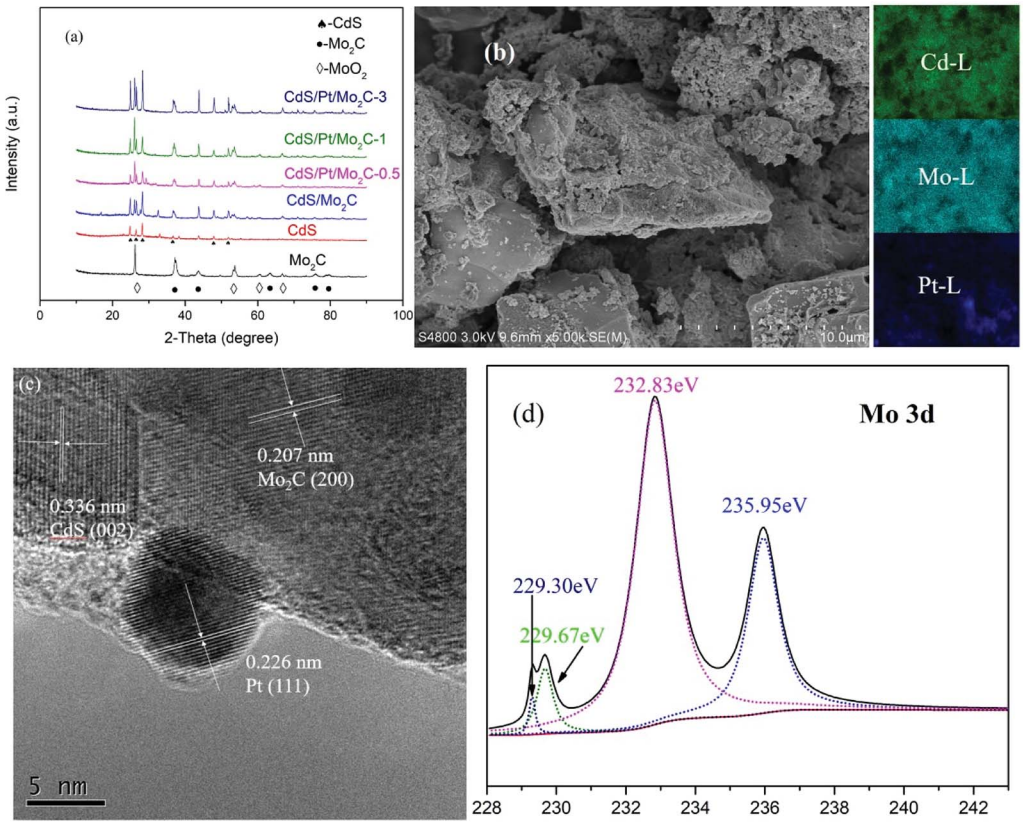

Fig. 1 (a) XRD patterns of all samples. (b) SEM image and elemental mapping patterns. (c) HRTEM images of the CdS/Pt/Mo_2C-0.5 sample. (d) The XPS peaks of Mo 3d of CdS/Pt/Mo_2C-0.5.

photogenerated electron–hole pairs (Fig. 2a). The PL spectra of different samples (Fig. 2b) over a wavelength range from 410 to 800 nm showed a strong peak at nearly 465 nm while the PL intensity decreased as: CdS > CdS/Mo_2C > Mo_2C > CdS/Pt/Mo_2C-3 > CdS/Pt/Mo_2C-1 > CdS/Pt/Mo_2C-0.5, as confirmed by EIS analysis (Fig. S2†). The PL intensity of the CdS/Mo_2C is much lower than that of CdS, indicating efficient electron transfer in the CdS/Mo_2C system from CdS to Mo_2C, leading to the spatial separation of electrons and holes. This phenomenon can be attributed to the inspiring separation process of electron–hole pairs connected with the metal character of Mo_2C. Furthermore, compared with CdS/Mo_2C, the CdS/Pt/Mo_2C system results in lower quenching of the PL intensity. The outcome of PL spectroscopy signifies that the photo-excited electrons transfer from CdS to Mo_2C, and then migrate to Pt under visible light irradiation.[24,25] The much higher transient photocurrent response also confirms the more efficient electron–hole separation for CdS/Pt/Mo_2C-0.5 in relation to the pure CdS and Mo_2C (Fig. 2c).[26] The EIS results of CdS and CdS/Pt/Mo_2C-0.5 (Fig. 2d) also prove that the conductivity of CdS/Pt/Mo_2C-0.5 is much better than that of CdS.

The optical properties of different samples were investigated by UV-vis diffuse reflection spectroscopy (DRS). An obvious enhancement, compared with that of CdS, in the absorption of wavelengths longer than 530 nm is seen in CdS/Mo_2C based on the UV-vis spectrum (Fig. 2e). The corresponding main band structures of the different samples (Fig. S4a†) in visible light region are calculated by the transformed Kubelka–Munk function $\alpha h\nu = A(h\nu - E_g)^2$. The valence band potentials (Fig. S4b†) are 1.25, 0.99, 1.8, 1.05, 1.49 eV for CdS, CdS/Mo_2C, CdS/Pt/Mo_2C-0.5, CdS/Pt/Mo_2C-1 and CdS/Pt/Mo_2C-3, respectively. More clearly, the band positions of E_{CB} and E_{VB} for the different samples are illustrated in Fig. 2f. It can be found that the valence band and conduction band positions of CdS/Pt/Mo_2C-0.5 shift from 1.25 eV to 1.8 eV and from −0.63 eV to −0.07 eV, respectively, compared with those of CdS, which can be due to the SPR effect of Pt nanoparticles.[27] The results of optical test indicate the heterostructure system can efficiently improve the reductive capacity of the photo-generated electrons and significantly increase the photocatalytic activity of CdS.

The photocatalytic H_2 evolution in response to visible-light were examined for all samples in the presence of Na_2S (0.1 M) and Na_2SO_3 (0.1 M) as the sacrificial agent of the hole and the results are illustrated in Fig. 3a. The CdS/Pt/Mo_2C-0.5 shows the best H_2 evolution performance with a rate of 1828.82 μmol h^{-1} g^{-1}, which is 8.5 times and 16.2 times higher than that of pure CdS and CdS/Mo_2C, respectively. Compared with other samples, CdS/Pt/Mo_2C-0.5 possesses apparent quantum yield of 9.39% (AQY = 9.39%) under visible-light irradiation.[25,28–33] Interestingly, upon further increasing the percent of Pt nanoparticles, the rate for photocatalytic hydrogen generation decreases, which is probably due to the extra percent of Pt nanoparticles in the CdS/Pt/Mo_2C system. The excessive Pt may act as the center of recombination, which has been proven by previous

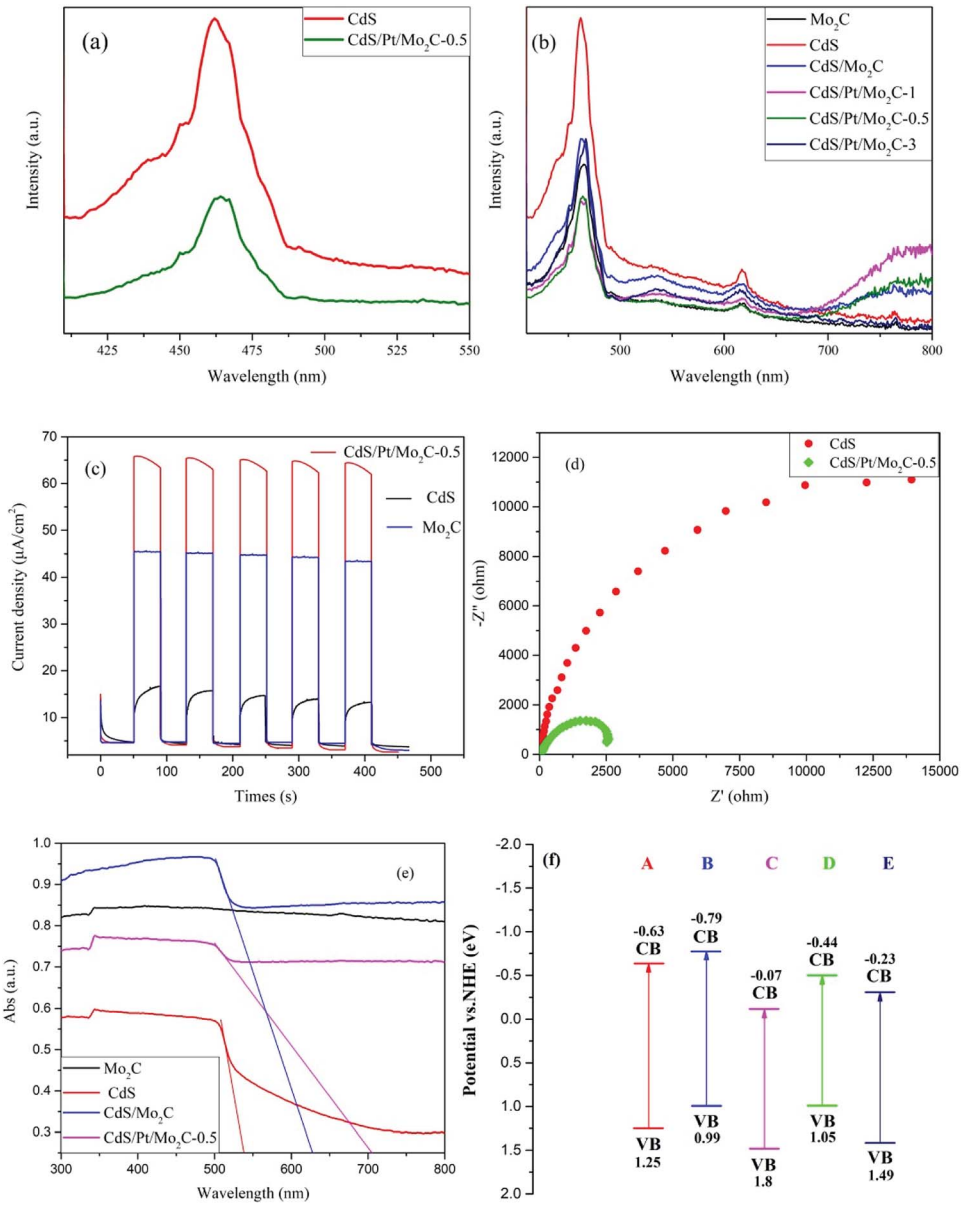

Fig. 2 (a) PL spectra of the pure CdS nanoparticles and CdS/Pt/Mo_2C-0.5. (b) PL spectra of different samples. (c) Transient photocurrent response of the pure CdS nanoparticles, Mo_2C and CdS/Pt/Mo_2C-0.5. (d) EIS Nyquist plots of CdS and CdS/Pt/Mo_2C-0.5 samples. (e) DRS spectra of Mo_2C, CdS and CdS/Pt/Mo_2C-0.5. (f) Schematic illustration of band structures of the different samples *vs.* NHE, (A) CdS, (B) CdS/Mo_2C, (C) CdS/Pt/Mo_2C-0.5, (D) CdS/Pt/Mo_2C-1 and (E) CdS/Pt/Mo_2C-3.

research.[20] The photocatalytic activity of the noble-metal-based CdS/Pt photocatalyst was also explored and an optimal H_2 evolution rate of 566.32 μmol h^{-1} g^{-1} was obtained (Fig. S7†). Taking the H_2 evolution rate of CdS/Pt/Mo_2C-0.5 is 1828.82 μmol h^{-1} g^{-1} into consideration, which can prove that Mo_2C can be used to boost the photo-activity. The role of CdS in the CdS/Pt/Mo_2C system, as proven by the photocatalytic activity tests, was that of a photocatalyst. At the same time Pt nanoparticles were acting as the photosensitizer and activity sites.

In order to verify the stability of the photocatalyst, an experiment to determine the recyclability of CdS and CdS/Pt/Mo_2C-0.5 was carried out (Fig. 3b). From Fig. 3b, it can be observed that CdS/Pt/Mo_2C-0.5 shows excellent stable performance under visible-light irradiation, and there is almost no significant decrease in the amount of photocatalytic H_2 evolution for CdS/Pt/Mo_2C-0.5, compared with that of CdS. The results confirm that CdS/Pt/Mo_2C-0.5 is a robust photocatalyst. In addition, XRD and SEM analyses of fresh and used samples (Fig. S8 and S9†) reveal that there is no obvious difference between the two samples regarding composition and microstructure, which indicates that the CdS/Pt/Mo_2C-0.5 is a stable catalyst under the designed reaction conditions.

3.1 Photocatalytic mechanism of the CdS/Pt/Mo_2C system

On the basis of the above experimental results and discussions, a possible mechanism for H_2 evolution under visible-light in the

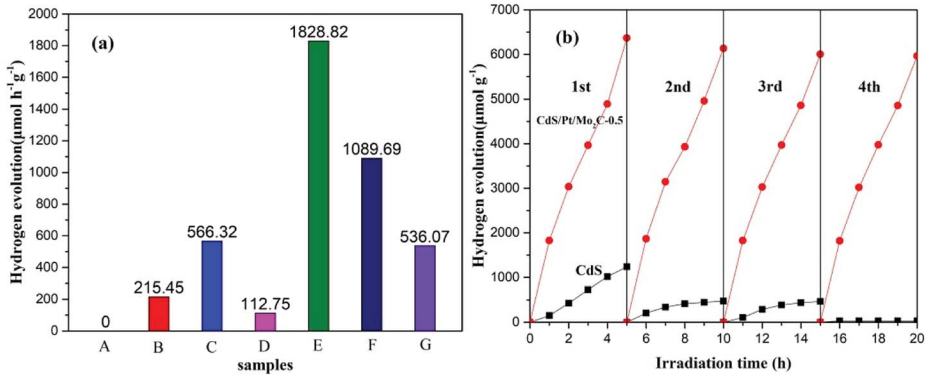

Fig. 3 (a) Hydrogen evolution rate of different samples in 0.1 M Na_2S and 0.1 M Na_2SO_3 aqueous solution under visible light irradiation ($\lambda \geq 400$ nm); (A) Mo_2C, (B) CdS, (C) Pt/Mo_2C, (D) CdS/Mo_2C, (E) CdS/Pt/Mo_2C-0.5, (F) CdS/Pt/Mo_2C-1, (G) CdS/Pt/Mo_2C-3. (b) Recyclability testing and comparison of H_2 evolution over CdS and CdS/Pt/Mo_2C-0.5 in 0.1 M Na_2S and 0.1 M Na_2SO_3 aqueous solution as sacrificial reagents.

CdS/Pt/Mo_2C system is shown in Scheme 2. The enhanced photocatalytic activity H_2 evolution of CdS/Pt/Mo_2C under visible-light condition could be attributed to the introduction of Pt nanoparticles and Mo_2C, which created narrow bandgap energy and excellent separation efficiency of photo-generated electrons–holes. This consequently improved the absorption region of photocatalyst and improved charge carrier separation. Owing to the close connection of heterostructures and excellent separation of photo-generated electrons and holes caused by the metal character of Mo_2C, the CdS/Pt/Mo_2C heterostructure showed enhanced photocatalytic activity for hydrogen production under visible-light irradiation, compared with CdS and Pt/Mo_2C. When irradiated by visible-light, CdS generates electron–hole pairs and the electrons are exited into the conduction band and then injected into Mo_2C. The photogenerated electrons can be efficiently transferred to Pt nanoparticles where hydrions are reduced in the presence of the photogenerated electrons to produce H_2. The hole left on the valence band of CdS reacts with the electron donor (Na_2S/Na_2SO_3).

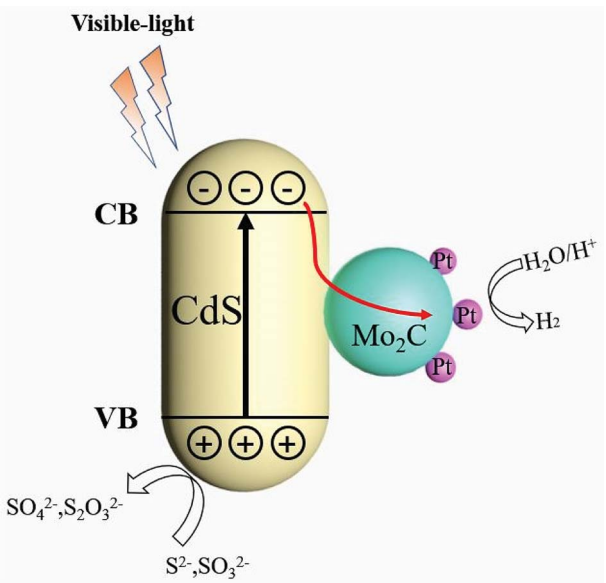

Scheme 2 Photocatalytic mechanism of CdS/Pt/Mo_2C system under visible-light irradiation (λ > 400 nm).

4. Conclusion

In summary, triphase CdS/Pt/Mo_2C heterostructure is a highly efficient and wide-spectrum-responsive photocatalyst. The investigation of the visible-light photocatalytic properties of the CdS/Pt/Mo_2C composites shows a high photoactivity with H_2 evolution rate of 1828.82 μmol h^{-1} g^{-1} and AQY of 9.39%. The aim of decreasing the amount of Pt used in the photocatalyst and increasing the activity of the photocatalyst was achieved, as proven by the optimal H_2 evolution rate of 566.32 μmol h^{-1} g^{-1} in Pt/CdS. The superior performance can be due to the excellent separation of photo-generated electrons and holes and the electron transfer efficiency caused by the metal character of Mo_2C which can not only inhibit the recombination of the photo-generated electron–hole pairs but also increase the visible-light absorption in CdS. Mo_2C may provide some insight into the construction of novel and significantly efficient heterostructure photocatalysts for practical utilization in solar energy.

Conflicts of interest

There are no conflicts to declare.

Acknowledgements

The work was supported by the National Natural Science Foundation of China (grant No. 21267020).

References

1 L. Lin, W. Zhou, R. Gao, S. Yao, X. Zhang, W. Xu, S. Zheng, Z. Jiang, Q. Yu, Y.-W. Li, C. Shi, X.-D. Wen and D. Ma, *Nature*, 2017, DOI: 10.1038/nature21672.
2 Y. Shi and B. Zhang, *Chem. Soc. Rev.*, 2016, **45**, 1529–1541.

3 H. Maleki and N. Hüsing, *Appl. Catal., B*, 2018, **221**, 530–555.
4 X. Sheng, Z. Liu, R. Zeng, L. Chen, X. Feng and L. Jiang, *J. Am. Chem. Soc.*, 2017, **139**, 12402–12405.
5 M. Parasram and V. Gevorgyan, *Chem. Soc. Rev.*, 2017, **46**, 6227–6240.
6 J. Ferreira de Brito, F. Tavella, C. Genovese, C. Ampelli, M. V. B. Zanoni, G. Centi and S. Perathoner, *Appl. Catal., B*, 2018, **224**, 136–145.
7 H. Mou, C. Song, Y. Zhou, B. Zhang and D. Wang, *Appl. Catal., B*, 2018, **221**, 565–573.
8 H. Shi, Y. Yu, Y. Zhang, X. Feng, X. Zhao, H. Tan, S. U. Khan, Y. Li and E. Wang, *Appl. Catal., B*, 2018, **221**, 280–289.
9 C. Xue, S. Hu, Q. Chang, Y. Li, X. Liu and J. Yang, *RSC Adv.*, 2017, **7**, 49759–49768.
10 Z. Fang, S. Weng, X. Ye, W. Feng, Z. Zheng, M. Lu, S. Lin, X. Fu and P. Liu, *ACS Appl. Mater. Interfaces*, 2015, **7**, 13915–13924.
11 Y. Qu and X. Duan, *Chem. Soc. Rev.*, 2013, **42**, 2568–2580.
12 A. Celzard, J. F. Marêché, G. Furdin, V. Fierro, C. Sayag and J. Pielaszek, *Green Chem.*, 2005, **7**, 784.
13 N. M. Schweitzer, J. A. Schaidle, O. K. Ezekoye, X. Pan, S. Linic and L. T. Thompson, *J. Am. Chem. Soc.*, 2011, **133**, 2378–2381.
14 J.-S. Li, Y. Wang, C.-H. Liu, S.-L. Li, Y.-G. Wang, L.-Z. Dong, Z.-H. Dai, Y.-F. Li and Y.-Q. Lan, *Nat. Commun.*, 2016, **7**, 11204.
15 R. Ma, Y. Zhou, Y. Chen, P. Li, Q. Liu and J. Wang, *Angew. Chem., Int. Ed.*, 2015, **54**, 14723–14727.
16 H. B. Wu, B. Y. Xia, L. Yu, X.-Y. Yu and X. W. Lou, *Nat. Commun.*, 2015, **6**, 6512.
17 W.-F. Chen, S. Iyer, S. Iyer, K. Sasaki, C.-H. Wang, Y. Zhu, J. T. Muckerman and E. Fujita, *Energy Environ. Sci.*, 2013, **6**, 1818–1826.
18 B. Zhu, L. Zhang, B. Cheng and J. Yu, *Appl. Catal., B*, 2018, **224**, 983–999.
19 Y.-N. Liu, C.-C. Shen, N. Jiang, Z.-W. Zhao, X. Zhou, S.-J. Zhao and A.-W. Xu, *ACS Catal.*, 2017, **7**(12), 8228–8234.
20 B. Ma, H. Xu, K. Lin, J. Li, H. Zhan, W. Liu and C. Li, *ACS Sustainable Chem. Eng.*, 2016, **9**, 820–824.
21 A. A. Ismail and D. W. Bahnemann, *Sol. Energy Mater. Sol. Cells*, 2014, **128**, 85–101.
22 Z. Xing, J. Zhang, J. Cui, J. Yin, T. Zhao, J. Kuang, Z. Xiu, N. Wan and W. Zhou, *Appl. Catal., B*, 2018, **225**, 452–467.
23 Z. Zhao, G. Ge and D. Zhang, *ChemCatChem*, 2018, **10**, 62–123.
24 W. Zhao, L. Xie, M. Zhang, Z. Ai, H. Xi, Y. Li, Q. Shi and J. Chen, *Int. J. Hydrogen Energy*, 2016, **41**, 6277–6287.
25 D. Jiang, X. Chen, Z. Zhang, L. Zhang, Y. Wang, Z. Sun, R. M. Irfan and P. Du, *J. Catal.*, 2017, **357**, 147–153.
26 P. Xiao, J. Lou, H. Zhang, W. Song, X.-L. Wu, H. Lin, J. Chen, S. Liu and X. Wang, *Catal.: Sci. Technol.*, 2018, **8**, 201–209.
27 P. Zhou, J. Yu and M. Jaroniec, *Adv. Mater.*, 2014, **26**, 4920–4935.
28 Z. B. Yu, Y. P. Xie, G. Liu, G. Q. Lu, X. L. Ma and H.-M. Cheng, *J. Mater. Chem. A*, 2013, **1**, 2773–2776.
29 J. L. DiMeglio and B. M. Bartlett, *Chem. Mater.*, 2017, **29**, 7579–7586.
30 X. Guo, Y. Chen, Z. Qin, J. Su and L. Guo, *ChemCatChem*, 2018, **10**, 153–158.
31 P. Wang, Y. Sheng, F. Wang and H. Yu, *Appl. Catal., B*, 2018, **220**, 561–569.
32 F. Wang, Y. Wang, Y. Feng, Y. Zeng, Z. Xie, Q. Zhang, Y. Su, P. Chen, Y. Liu, K. Yao, W. Lv and G. Liu, *Appl. Catal., B*, 2018, **221**, 510–520.
33 Y. Zhang, Z. Peng, S. Guan and X. Fu, *Appl. Catal., B*, 2018, **224**, 1000–1008.